Pergamon

Int. J. Multiphase Flow Vol. 24, No. 1, pp. 17–34, 1998

Printed in Great Britain
0301-9322/98 $19.00 + 0.00

PII: S030-9322(97)00041-4

STABILITY OF SMALL DIAMETER AIRLIFT PUMPS

F. DE CACHARD† and J. M. DELHAYE

Commissariat à l'Energie Atomique/Grenoble, Département de Thermohydraulique et de Physique, 38054 Grenoble Cedex 9, France

(Received 15 October 1996; in revised form 22 May 1997)

Abstract—In an airlift pumping process, air is injected into the pipe containing the fluid to be transferred. Small diameter airlift pumps are, in particular, used for corrosive or radioactive liquids. However, for certain combinations of the geometrical parameters and air flow rate, they may become unstable. In this case, the flow at the riser outlet pulsates strongly, which cannot be accepted for many applications.

An airlift pump involves three different regions, e.g. a single phase liquid flow and a separate single phase gas flow upstream of the air injection device and a two-phase flow downstream. The instabilities are due to density wave oscillations in the two-phase flow. Depending on the liquid flow inertia, friction effects and gas flow compressibility, the density waves are sustained or not.

The present study is based upon a detailed description of the steady state flow in a small diameter airlift pump. A linear stability analysis is performed and assessed against an extensive set of experimental data. Both the experimental and analytical results show that the influencing parameters have complex effects and strongly interact: the same variation of a parameter may have opposite effects, i.e. stabilizing or destabilizing, depending on the values of the other parameters. The effect of the compressibility of the gas flow between the regulating valve and the air-injection device is shown to be very important.

The analysis presented leads to a numerical model that can be considered as a practical tool for airlift performance and stability analysis. © 1997 Elsevier Science Ltd

Key Words: airlift pumps, stability, two-phase flow

1. INTRODUCTION

A detailed study of stable operation of small-diameter airlift pumps has been published previously (de Cachard and Delhaye 1996). This paper is the continuation of this study and deals with the prediction of instabilities. The reader should refer to the first paper for the description of the airlift pumps investigated (figure 1), the context, notation, and steady-state equations.

Unstable airlift operation involves low frequency (less than 1 Hz) oscillations of the liquid flow at the pump outlet. In the worst cases, the flow takes the form of violent, periodic expulsion of liquid jets.

The instabilities result from density wave oscillations in the riser, coupled with oscillations of the single phase liquid flow upstream of the air injection. Their basic mechanism has been explained by Hjalmars (1973), who also proposed a stability criterion based on the linear analysis of the transient flow equations. However, the two-phase flow model used, i.e. a homogeneous model without friction, was very crude.

A more complex version of Hjalmars' model including gas–liquid relative velocity has been proposed by Apazidis (1985). In this model a bubble flow with a uniform and imposed *initial* bubble diameter was assumed and the wall friction was still neglected. Both assumptions are unrealistic for small-diameter airlift pumps.

Moreover, Hjalmars and Apazidis assume that the air injection takes place near the bottom of a riser which is immersed in a large liquid tank. When the liquid is supplied to the air-injection zone through a pipe, the geometrical parameters, e.g. length and diameter, of this pipe strongly influence the liquid flow inertia and, as a consequence, the system stability.

†Present address: Thermal-Hydraulics Laboratory, Paul-Scherrer Institute, CH-5232 Villigen-PSI, Switzerland.

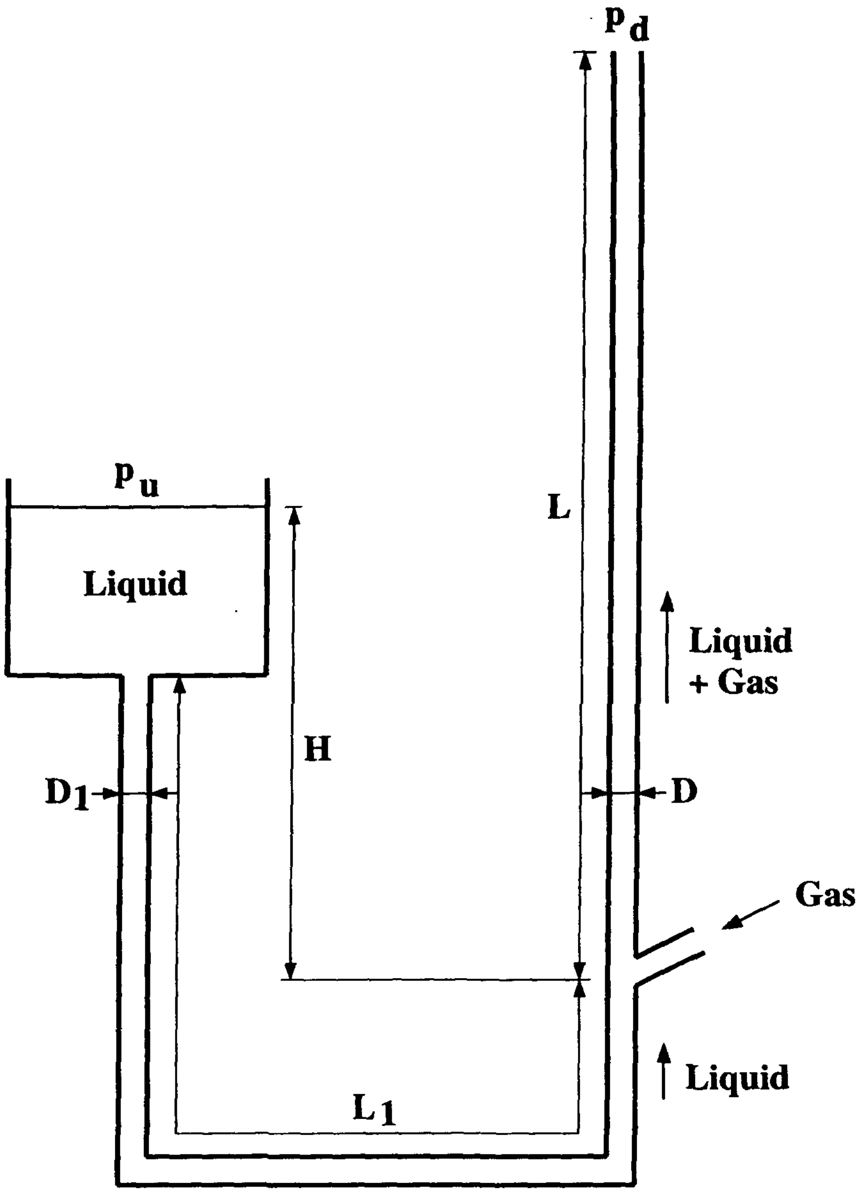

Figure 1. Typical airlift geometry. D, D_1: internal diameters of the riser and of the liquid suction pipe, respectively; p_u, p_d: upstream and downstream pressure; S: submergence, defined as H/L.

Finally, the influence of the gas supply pipe, between the regulating valve and the air injection, was not accounted for. Gas compressibility effects, directly related to the volume of the gas supply pipe, have a very strong destabilizing influence. These effects cannot be avoided in many cases, e.g. when airlift pumps are used for radioactive liquids, the regulating valves having to be kept outside the contaminated area.

Table 1. Test designation (bold) and parameters

			submergence (S)				
liquid	length (m)	diameter (mm)	0.3		0.5		0.7
pipe	5.5 + 8S	19.4		**151**	**152**		
		9.2	**232**	**251**	**252**	**253**	**272**
	11.7 + 8S	9.2			**352**		
			29.6	6.9	29.6	54.6	29.6
			gas pipe length (m) (diameter: 10 mm)				

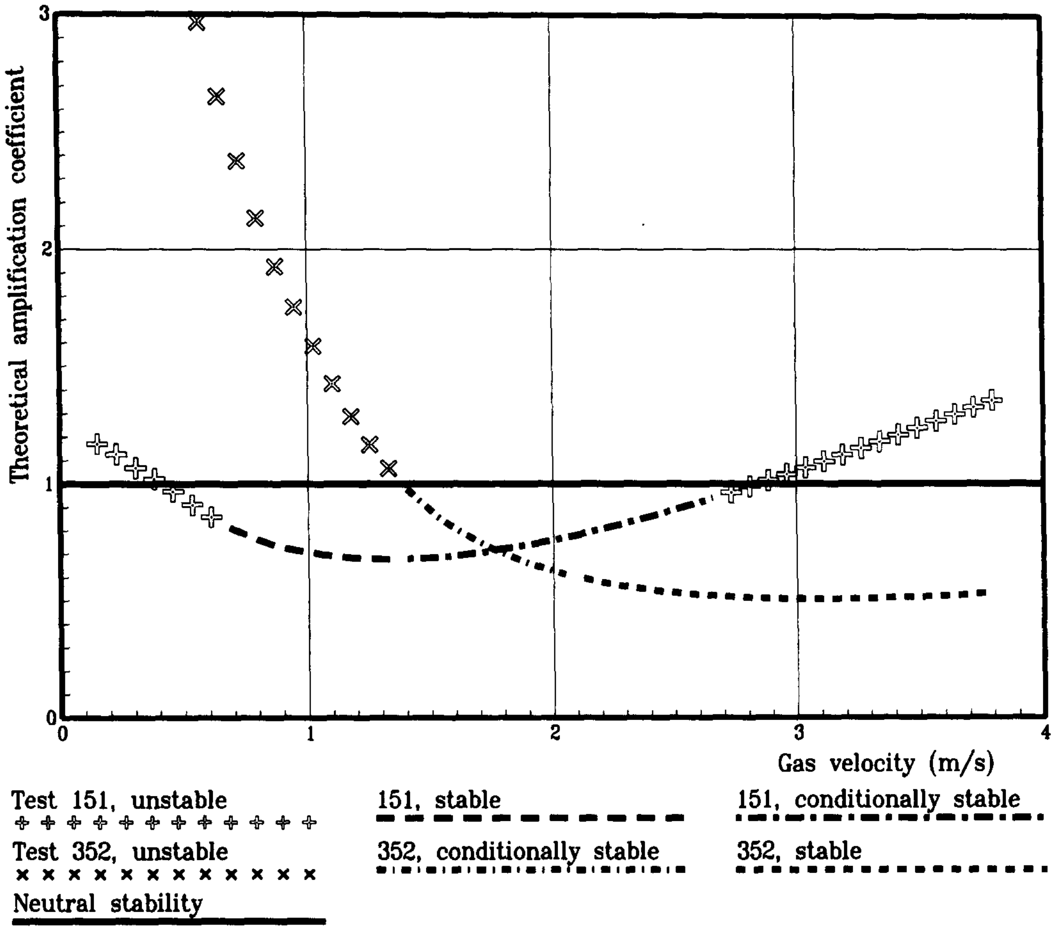

Figure 2. Examples of airlift stability curves: test 151 and 352 (data in table 1). The curves represent the results of the linear stability analysis. The experimental results appear through the symbols used to represent the calculated values (see legend). Lines are used when stable operation could be obtained, whereas symbols are used when the system was always unstable. The gas velocity corresponds to $M_G/(A\rho_{Gd})$, M_G being the injected gas mass flow rate, A the riser cross-sectional area, and ρ_{Gd} the gas density at the riser outlet.

A linear stability analysis is proposed hereafter, based on our steady-state model (de Cachard and Delhaye 1996) which includes a detailed description of the two-phase flow in the riser. The strong influences of the liquid and gas supply pipes are accounted for. The theoretical results are assessed against experimental results obtained for a large range of the influence parameters, i.e. the airlift submergence, gas flow rate, and liquid and gas pipe geometries.

The procedure used for the linear analysis is classical, and consists in:

—deriving the transient flow equations;
—splitting each variable X into

$$X = \bar{X} + \tilde{X} \qquad [1]$$

where $\bar{X}$ is the solution of the steady-state equations and $\tilde{X}$ the time-dependent perturbation;
—linearizing the flow equations in the case of small perturbations;
—analyzing the rate of growth for the perturbations.

The input parameters are defined in section 2.1 of the steady-state analysis, i.e. the air mass flow rate M_G, the geometrical parameters (H, L, L_1, D, D_1), the pressure conditions (p_v, p_d), the fluid physical properties, and also the gas pipe volume v_2 located between the air flow regulating valve and the injection tee.

2. ANALYSIS

2.1. *Transient flow equations*

2.1.1. *Single phase liquid flow*. The friction pressure losses are expressed using the steady-state relationships. The expression of the pressure just downstream from the tee (p_T), [9] in the steady-state model, must be complemented with the liquid inertia term

$$-\rho_L L_l \frac{d}{dt} J_{L_l} \qquad [2]$$

where L_l is the length of the liquid suction pipe and J_{L_l} the velocity in this pipe, given by

$$J_{L_l} = J_{LT} \frac{A}{A_l} \qquad [3]$$

where J_{LT} is the liquid superficial velocity just downstream of the tee, A and A_l being the riser and liquid suction pipe cross-sectional areas, respectively.

Hence

$$p_T = p_u + \rho_L g H - \mathscr{A} - \mathscr{B} \qquad [4]$$

with

$$\mathscr{A} \triangleq \rho_L \frac{A}{A_l} \frac{d}{dt} J_{LT} \qquad [5]$$

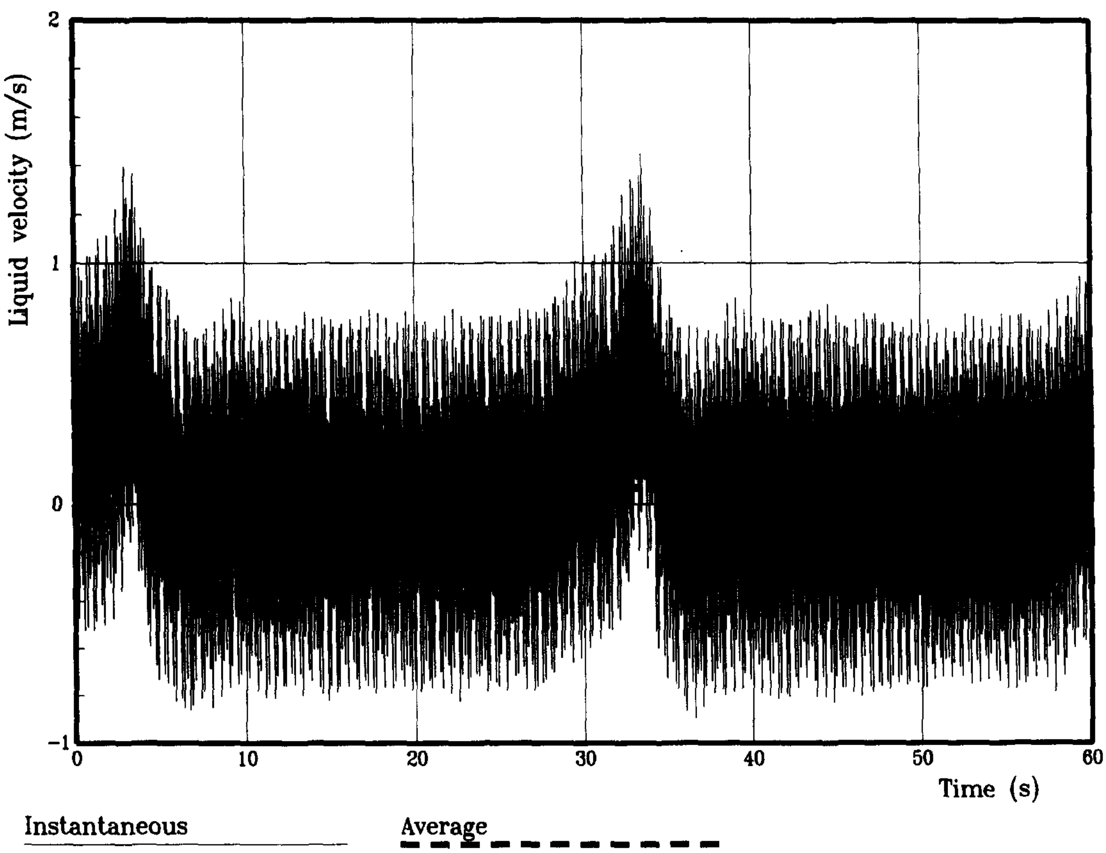

Figure 3(a).

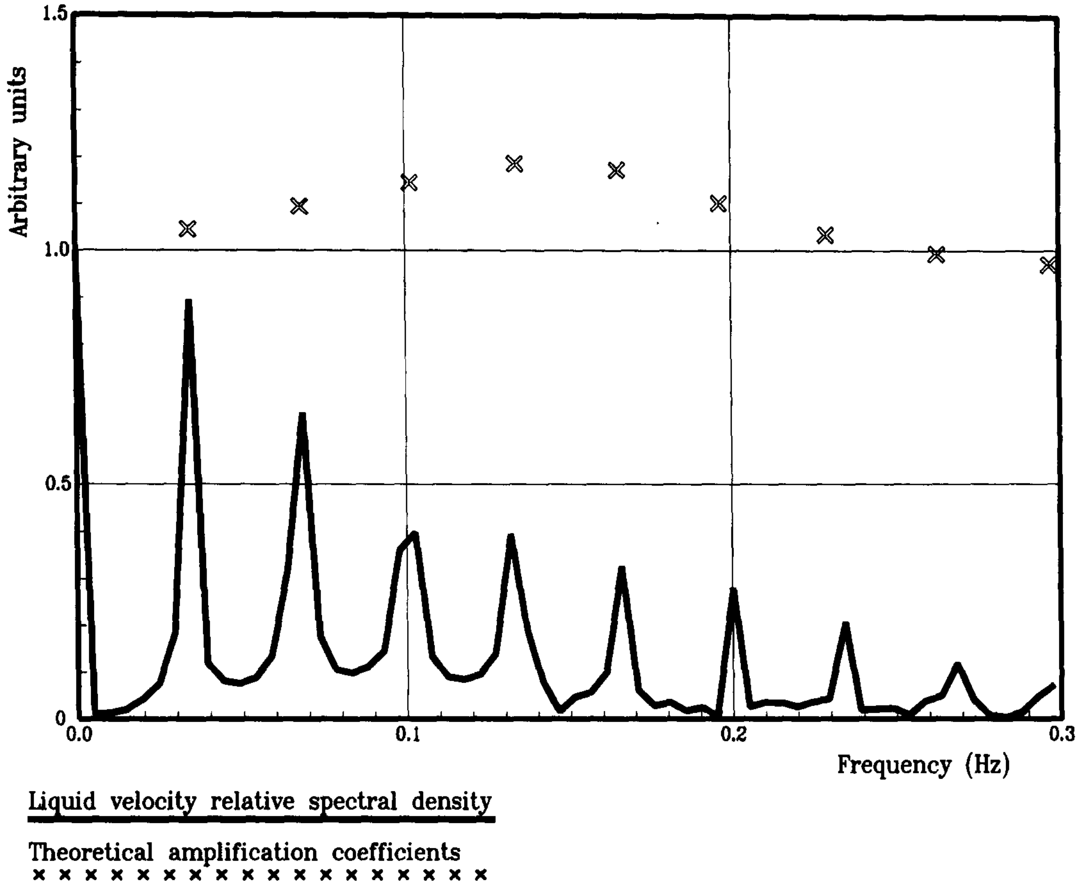

Figure 3(b).

Figure 3. Unstable operating point at low gas velocity. Liquid velocity time trace and relative spectral density for test 151 with $J_G = 0.15$ m/s. Comparison with frequencies and amplification coefficients corresponding to successive roots of [63]. The liquid velocity corresponds to the liquid flow rate in the suction pipe divided by the riser cross-sectional area.

$$\mathscr{B} \triangleq \frac{1}{2}\rho_L J_{LT}^2\left[\left(\lambda_l\frac{L_l}{D_l}+\zeta_l\right)\left(\frac{A}{A_l}\right)^2+(1+\zeta_c)\frac{1}{(1-\epsilon_T)^2}\right] \qquad [6]$$

where λ_l and ζ_l denote the friction factor and the sum of the singular pressure drop coefficients in the suction pipe, respectively, ζ_c the singular pressure drop coefficient corresponding to the liquid flow contraction in the air-injection zone, and ϵ_T the void fraction just downstream of the tee (the symbol $\triangleq$ is used for 'is defined as').

2.1.2. *Single phase gas flow.* The following assumptions are made:

—ideal gas;
—adiabatic flow;
—homogeneous pressure and temperature in the gas pipe: $p_T(t)$ and $\theta_T(t)$.

Neglecting the kinetic and potential energy terms, the total energy balance between the flow regulating valve and the tee reads

$$\frac{d}{dt}U_G = -\Delta(M_G h_G) \qquad [7]$$

where U_G is the (total) gas internal energy given by

$$U_G = c_{vG}\rho_{GT}v_2\theta_T \qquad [8]$$

c_{vG} being the gas specific heat at constant volume, ρ_{GT} the gas density, v_2 the volume of the gas pipe, h_G the gas specific enthalpy and M_G the gas mass flow rate.

The conditions at the flow regulating valve are

$$M_G = \bar{M}_G \text{ (choked flow)} \quad [9]$$

$$h_G = c_{pG}\theta_v \quad [10]$$

where c_{pG} denotes the gas specific heat at constant pressure and θ_v the gas temperature at the valve.

At the air-injection tee, the conditions are

$$M_G = \rho_{GT}J_{GT}A \quad [11]$$

$$h_G = c_{pG}\theta_T \quad [12]$$

where J_{GT} denotes the gas superficial velocity in the riser just downstream from the tee and A the riser cross-sectional area.

Hence

$$v_2 c_{vG} \frac{d}{dt}(\rho_{GT}\theta_T) = \bar{M}_G c_{pG}\theta_v - \rho_{GT}J_{GT}Ac_{pG}\theta_T. \quad [13]$$

The ideal gas law reads

$$\rho_{GT}\theta_T = p_T/r_G \quad [14]$$

where r_G denotes the gas specific constant.

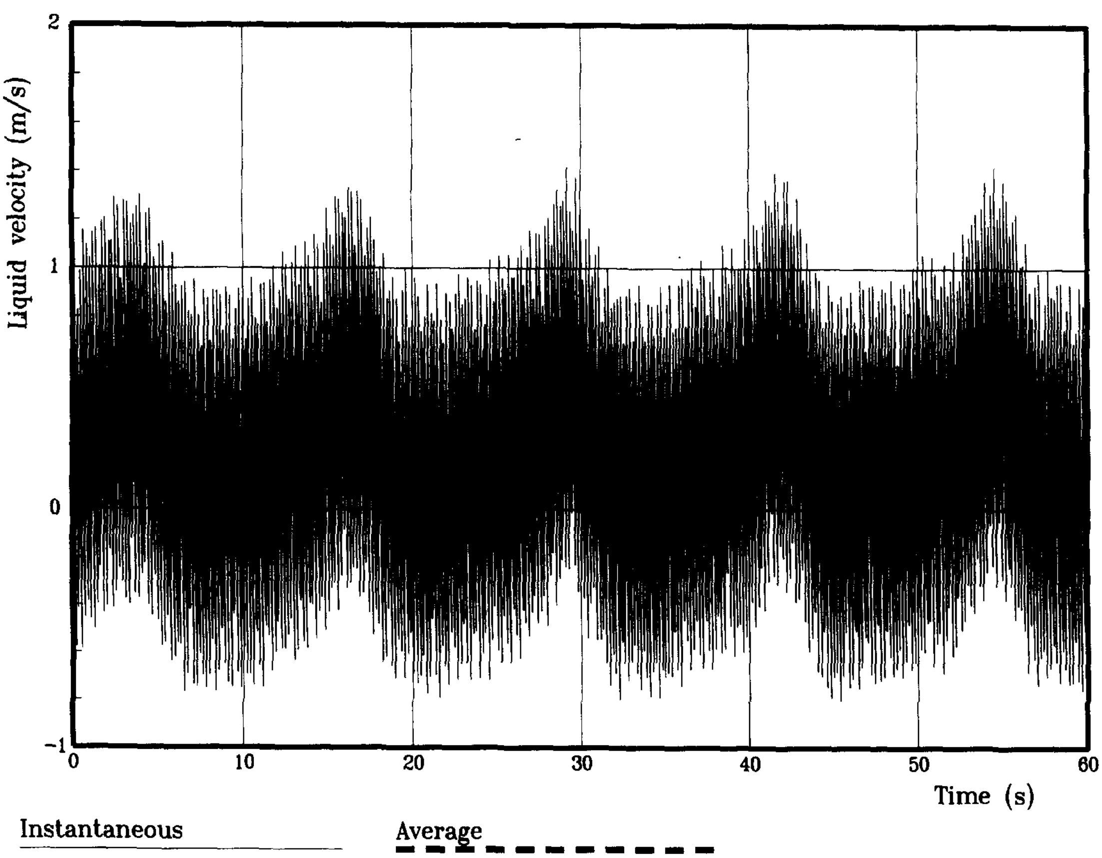

Figure 4(a).

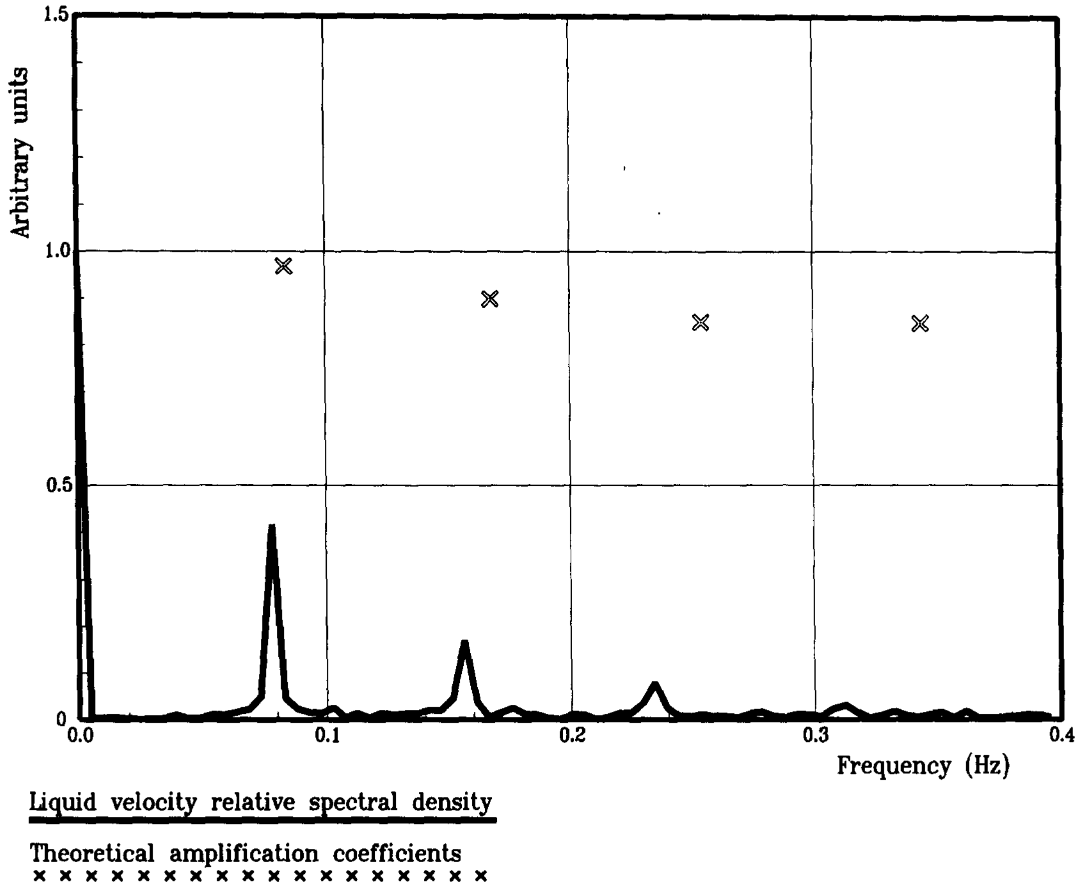

Figure 4(b).

Figure 4. Slightly unstable operating point at low gas velocity. Test 151; $J_G = 0.46$ m/s.

Combining the two previous equations leads to the following relation which describes the gas flow:

$$v_2 \frac{d}{dt} p_T + A\gamma J_{GT} p_T - \bar{M}_G \gamma r_G \theta_v = 0 \qquad [15]$$

with

$$\gamma \triangleq c_{pG}/c_{vG}. \qquad [16]$$

2.1.3. *Two phase flow.* The following assumptions and approximations are made.

—Gas density changes in the riser are accounted for in the steady-state reference solution (de Cachard and Delhaye 1996). However, in the time-dependent perturbation analysis, gas density is taken at the average pressure

$$\bar{p}_m = \frac{p_T + p_d}{2}. \qquad [17]$$

This first-order approximation is required to obtain a simple analytical solution for the void fraction ([35] below). It may be questionable for very tall airlift pumps (several tenths of metres).

—The rapid fluctuations of slug flow are not accounted for in the transient flow equations, which are written in terms of the averaged (over a short time) phase velocities and void fraction (V_G, V_L, ϵ). Indeed, the frequency ranges of the airlift instabilities and of the slug flow fluctuations are distinct (typically, 0.01 to 1 Hz in the first case, 1 to 20 Hz in the second one).

—The gas slip velocity and the wall friction term are expressed using the steady-state relationships.

The gas mass balance needs

$$\frac{\partial}{\partial t}(\rho_G \epsilon) = -\frac{\partial}{\partial z}(\rho_G J_G) \qquad [18]$$

where $\epsilon(z, t)$ is the void fraction and $J_G(z, t)$ the gas superficial velocity, with

$$J_G = \epsilon V_G \qquad [19]$$

V_G being the gas velocity.

The approximation $\rho_G = \bar{\rho}_G =$ constant yields

$$\frac{\partial}{\partial t}\epsilon + \frac{\partial}{\partial z}(\epsilon V_G) = 0. \qquad [20]$$

The mixture continuity equation reads

$$\frac{\partial}{\partial z} J = 0 \qquad [21]$$

where $J(t)$ denotes the mixture superficial velocity given by

$$J \triangleq J_G + J_L. \qquad [22]$$

The gas velocity is expressed, as in the steady-state, by

$$V_G = C_0 J + V_0 \qquad [23]$$

where the constants C_0 and V_0 are given by [25] and [28] to [32] of the steady-state model.

Since J is independent of z

$$\frac{\partial}{\partial z} V_G = 0 \qquad [24]$$

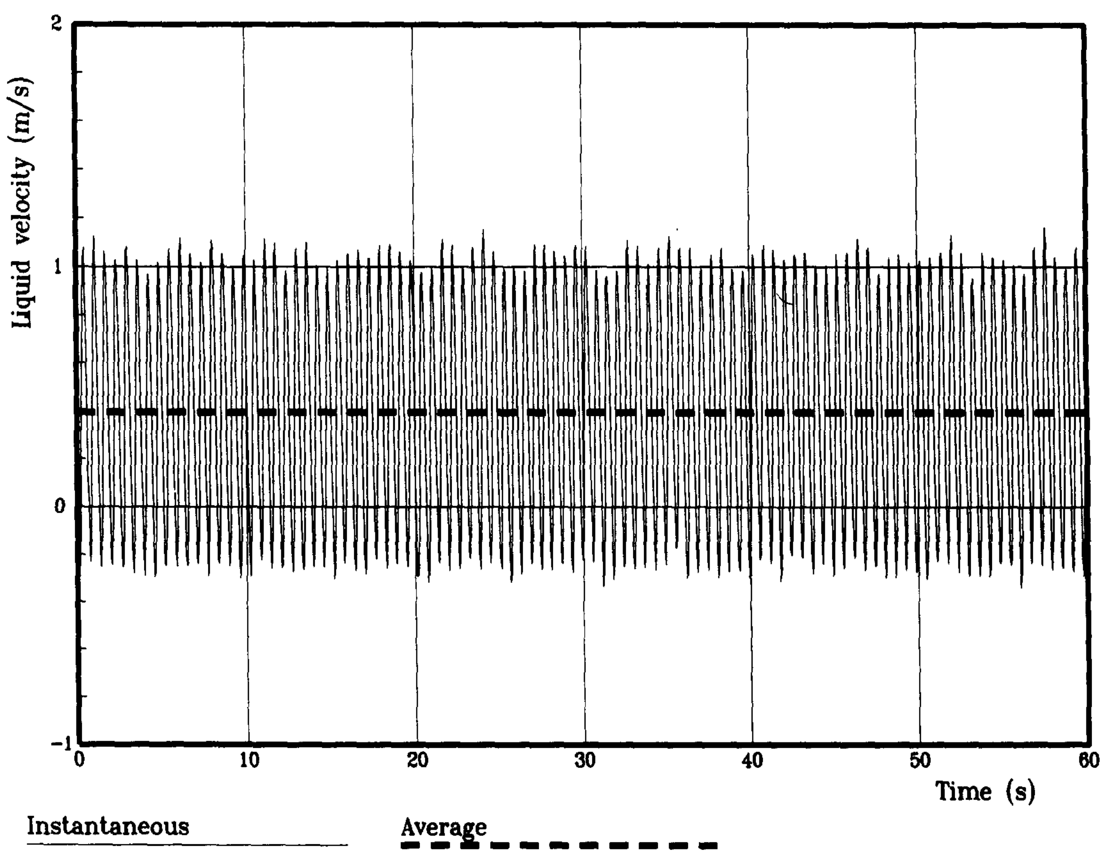

Figure 5(a).

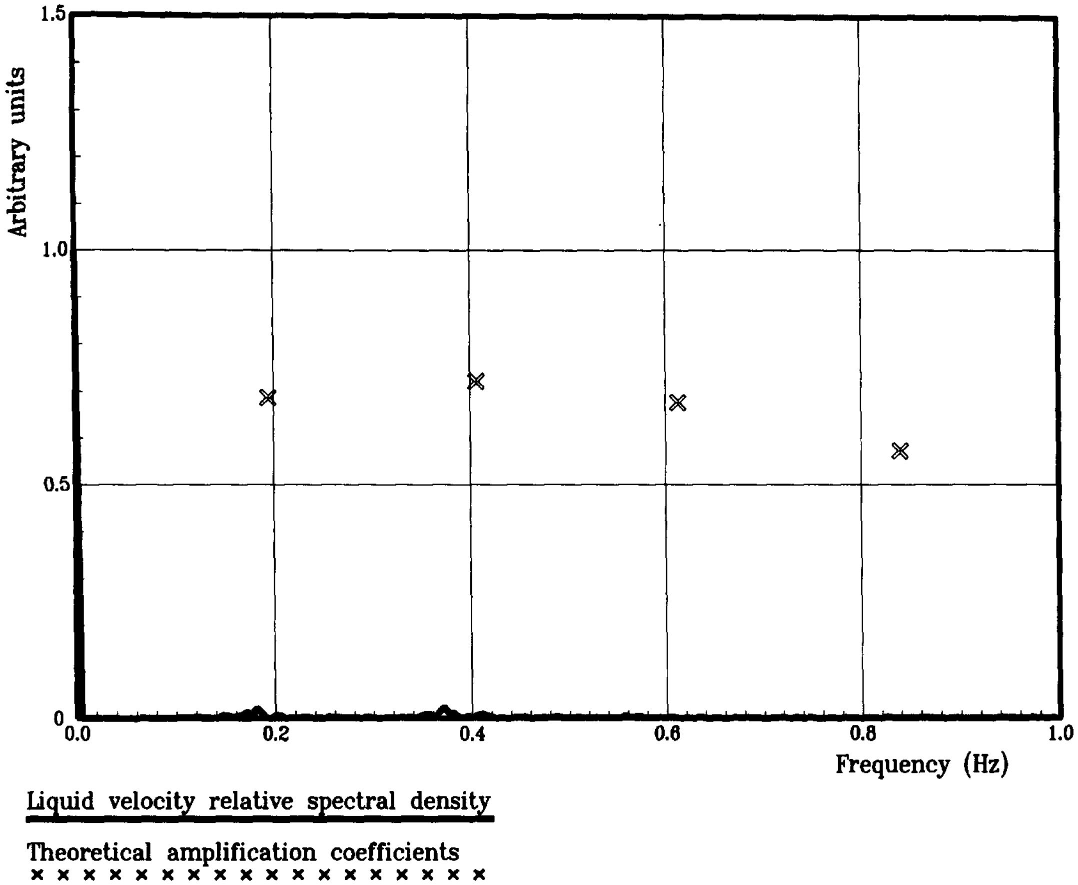

Figure 5(b).

Figure 5. (Conditionally) stable operating point. Test 151; $J_G = 1.52$ m/s; gas valve smoothly opened.

and the gas continuity equation [20] becomes

$$\frac{\partial}{\partial t}\epsilon + V_G(t)\frac{\partial}{\partial z}\epsilon = 0 \qquad [25]$$

which corresponds to void fraction propagation at velocity $V_G(t)$.

Neglecting as in steady-state, the gas inertia and gravity terms, the mixture momentum balance reads

$$\rho_L\frac{\partial}{\partial z}J_L + \rho_L\frac{\partial}{\partial z}\mathscr{M} + \frac{\partial}{\partial z}p - \mathscr{F} + \rho_L(1-\epsilon)g = 0 \qquad [26]$$

where $p(z, t)$ is the pressure and $\mathscr{M}$ the convection term, given by

$$\mathscr{M} \triangleq \frac{J_L^2}{1-\epsilon} \qquad [27]$$

$\mathscr{F}$ is the friction pressure gradient, given by the steady-state equations

$$\mathscr{F} = (1 - C_{\text{churn}})\mathrm{d}p/\mathrm{d}z)_{\text{f,slug}} + C_{\text{churn}}(\mathrm{d}p/\mathrm{d}z)_{\text{f,churn}} \qquad [28]$$

where $(\mathrm{d}p/\mathrm{d}z)_{\text{f,slug}}$ and $(\mathrm{d}p/\mathrm{d}z)_{\text{f,churn}}$ are the values predicted by the slug and churn flow models of the steady-state analysis (sections 3.2 and 3.3), and C_{churn} is an empirical interpolation coefficient (section 3.5).

2.1.4. *Summary*.The airlift transient behaviour is then described by [4], [15] (single-phase liquid and gas flow up to the mixing zone), [25], and [26] (two-phase flow: void propagation and momentum balance).

2.2. *Perturbations of the steady state*

The above equations are then linearized under the small perturbation approximation. The simple expression obtained for the void propagation equation enables the momentum balance to be integrated along the riser height by means of the method introduced by Hjalmars (1973). Eliminating $\tilde{p}_T$ (pressure at the tee) leads to two ordinary differential equations involving time-lag terms.

2.2.1. *Linearization of transient flow equations*. If Blasius' formula, given by [11] in the steady-state model, is used for λ_l, the linearized form of the liquid flow equation [4] reads

$$\tilde{p}_T(t) = -\rho_L L_l \frac{A}{A_l} \tilde{J}'_{LT}(t) - K_1 \tilde{J}_{LT}(t) - K_2 \tilde{\epsilon}_T(t) \qquad [29]$$

(J' denotes the derivative of J) with

$$K_1 \triangleq \rho_L \left[\bar{J}_L \left[\zeta_l \left(\frac{A}{A_l}\right)^2 + \frac{(1+\zeta_c)}{(1-\bar{\epsilon}_T)^2} \right] + 0.2765 \bar{J}_L^{0.75} D^{-1.25} \nu_L^{0.25} L_l \left(\frac{A}{A_l}\right)^{1.75} \right] \qquad [30]$$

$$K_2 \triangleq \rho_L \bar{J}_L^2 \frac{1+\zeta_c}{(1-\bar{\epsilon}_T)^3}. \qquad [31]$$

The gas equation [15] becomes

$$v_2 \tilde{p}'_T(t) + A\gamma[\bar{p}_T \tilde{J}_{GT}(t) + \bar{J}_{GT} \tilde{p}_T(t)] = 0. \qquad [32]$$

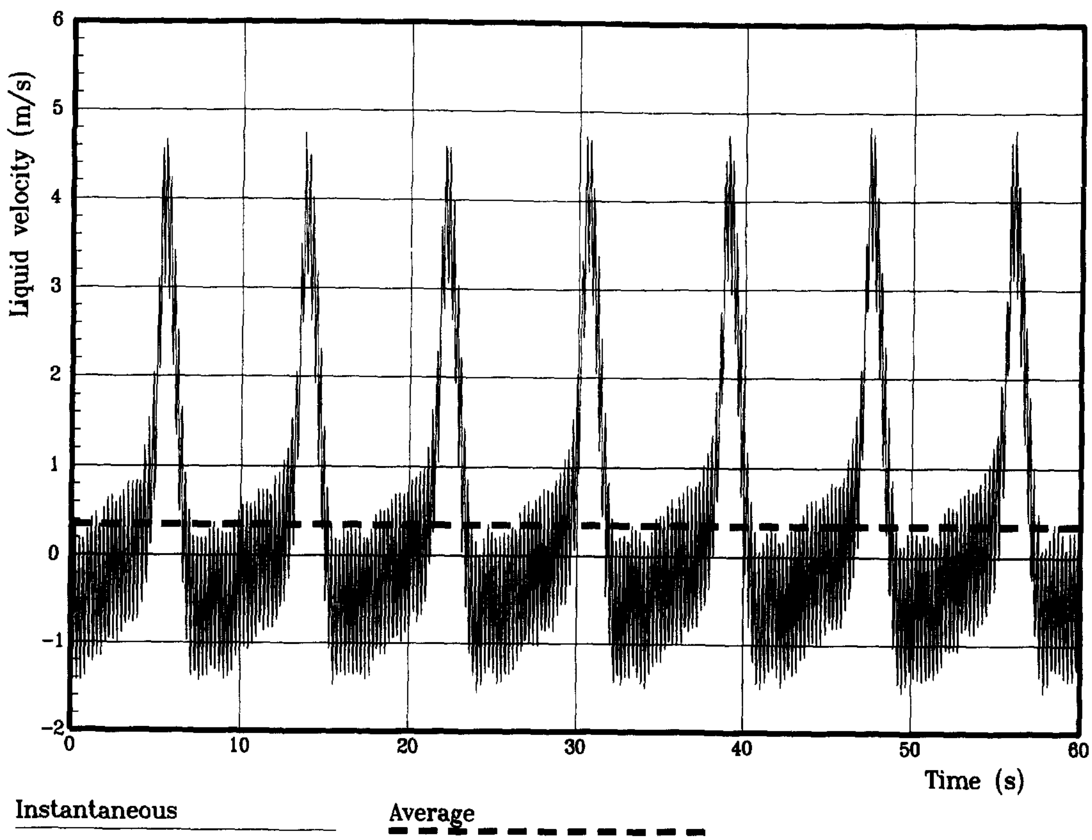

Figure 6(a).

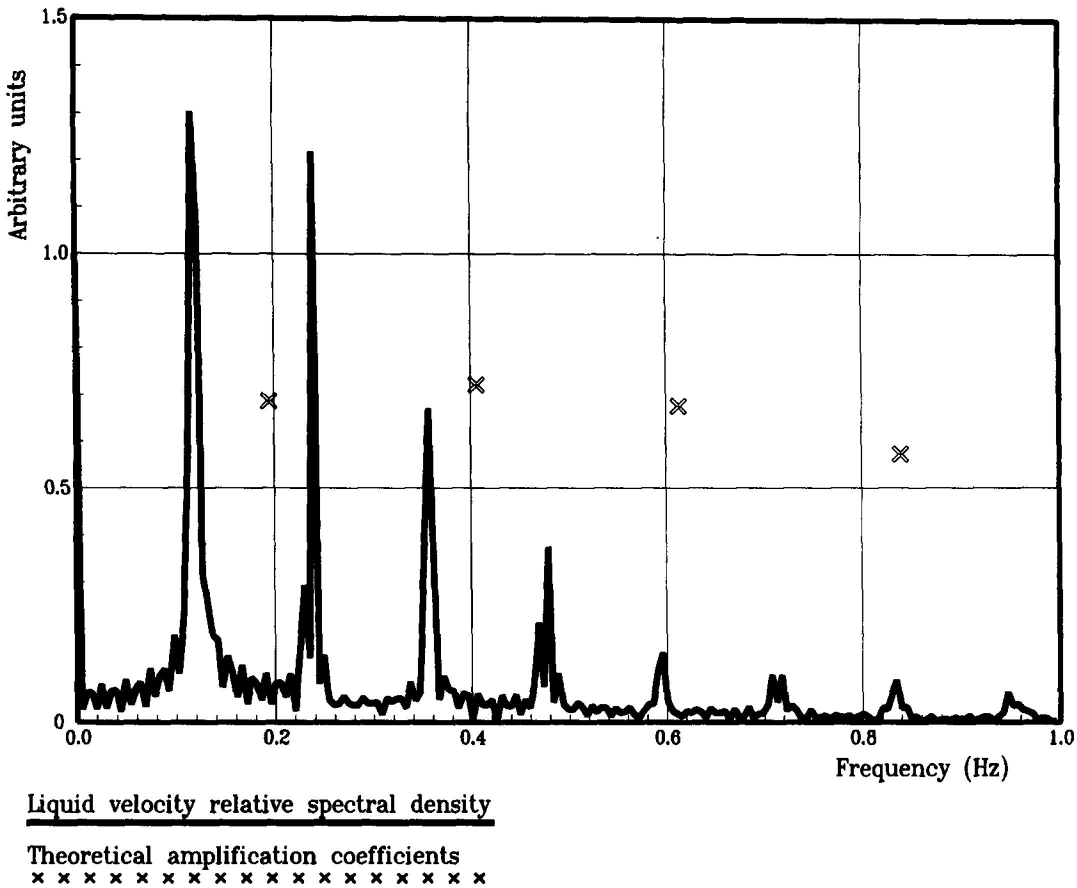

Figure 6(b).

Figure 6. Unstable operating point at high gas velocity. Test 151; $J_G = 1.52$ m/s reached from a higher value.

The void propagation equation [25] becomes

$$\frac{\partial}{\partial t}\tilde{\varepsilon} + \bar{V}_G \frac{\partial}{\partial z}\tilde{\varepsilon} = 0 \tag{33}$$

and the mixture momentum balance [26]

$$\rho_L \frac{\partial}{\partial t}\tilde{J}_L + \rho_L \frac{\partial}{\partial z}\tilde{\mathscr{M}} + \frac{\partial}{\partial z}\tilde{p} - \tilde{\mathscr{F}} + \rho_L g(1 - \tilde{\varepsilon}) = 0. \tag{34}$$

2.2.2. *Integration of momentum balance*. [33] corresponds to a propagation of the void perturbation $\tilde{\varepsilon}$ at constant velocity $\bar{V}_G$. $\tilde{\varepsilon}$ may thus be considered as a function of the variable $(t - z/\bar{V}_G)$ only. The following notation is used:

$$\tilde{\varepsilon} = f'(t - z/\bar{V}_G) \tag{35}$$

where f' denotes the derivative of f.

f' is integrated between the air-injection tee ($z = 0$) and the riser top ($z = L$):

$$\int_0^L f'(t - z/\bar{V}_G)\,\mathrm{d}z = \bar{V}_G[f(t) - f(t - T)] \tag{36}$$

where T is the gas transit time in the riser, given by

$$T = L/\bar{V}_G. \tag{37}$$

The perturbations of the two-phase flow variables are expressed as functions of $\tilde{\epsilon}$, $\tilde{J}$, and $\tilde{p}$, using the drift–flux relationships [19] and [23]. The following notation is used:

$$\tilde{J}(t) = g'(t). \qquad [38]$$

The expressions obtained for the superficial velocities are

$$\tilde{J}_{\mathrm{G}} = \bar{V}_{\mathrm{G}} f'(z, t) + C_0 \bar{\epsilon} g'(t) \qquad [39]$$

$$\tilde{J}_{\mathrm{L}} = -\bar{V}_{\mathrm{G}} f'(z, t) + (1 - C_0 \bar{\epsilon}) g'(t) \qquad [40]$$

and, for the convection and friction terms of the momentum balance

$$\tilde{\mathcal{M}} = M_1 f'(z, t) + M_2 g'(t) \qquad [41]$$

$$\tilde{\mathcal{F}} = F_1 f'(z, t) + F_2 g'(t) \qquad [42]$$

with

$$M_1 \triangleq \bar{V}_{\mathrm{L}}^2 - 2\bar{V}_{\mathrm{G}} \bar{V}_{\mathrm{L}} \qquad [43]$$

$$M_2 \triangleq \frac{2(1 - C_0 \bar{\epsilon})\bar{J}_{\mathrm{L}}}{1 - \bar{\epsilon}} \qquad [44]$$

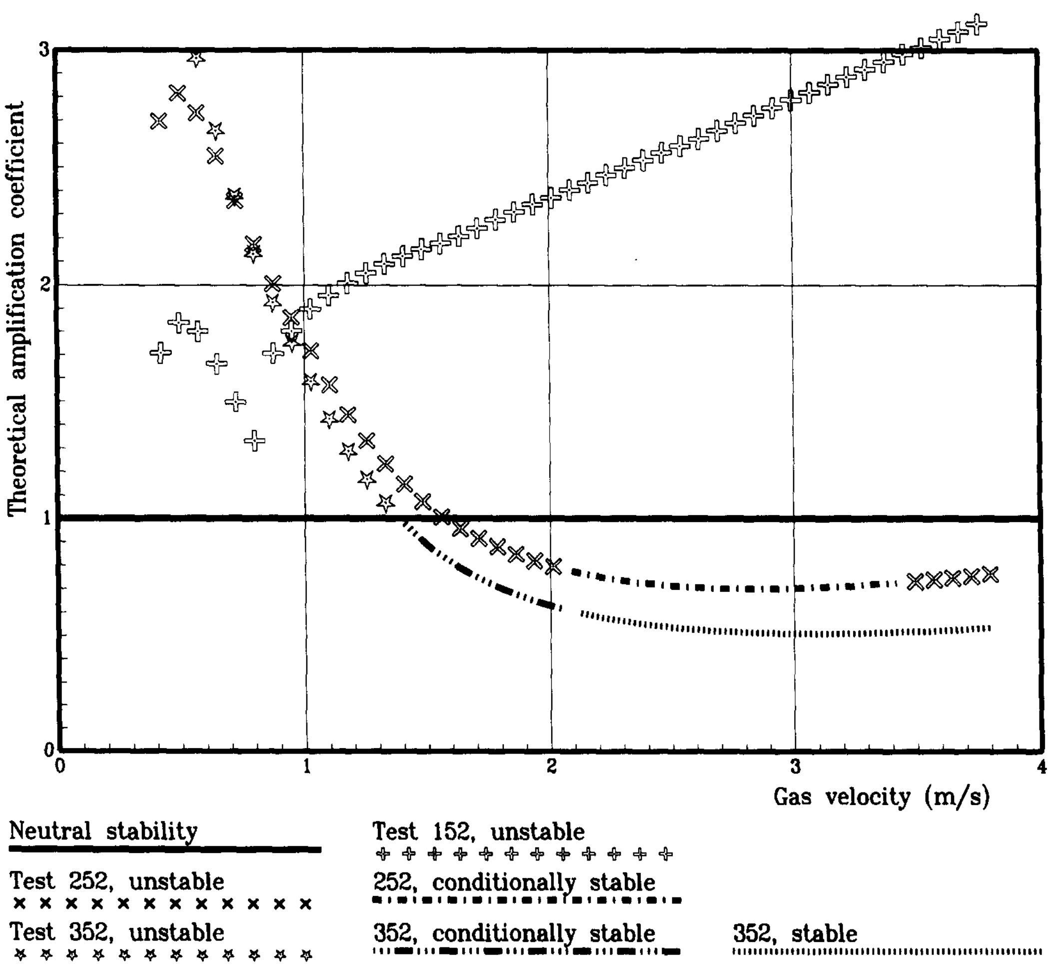

Figure 7. Effect of inertia and friction in the liquid suction pipe on airlift stability.

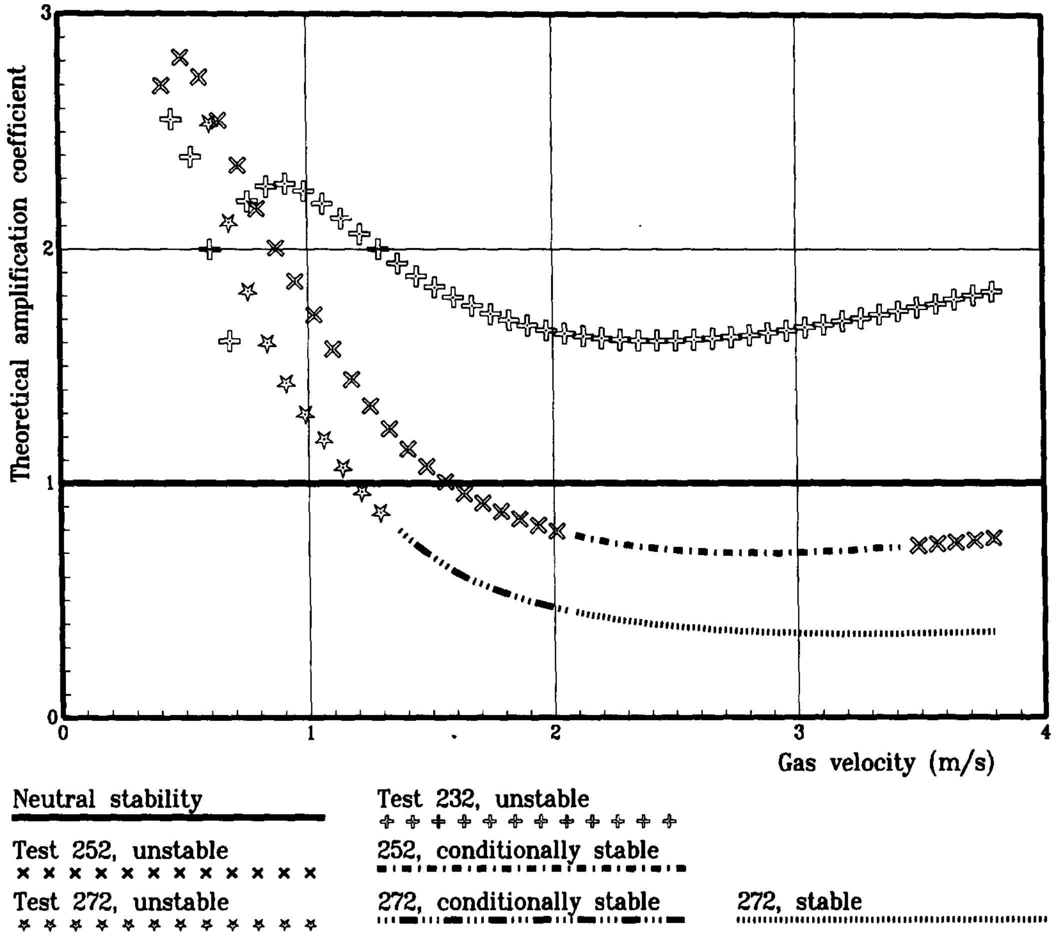

Figure 8. Effect of submergence on airlift stability.

$$F_1 \triangleq \left(\frac{\partial \mathscr{F}}{\partial \epsilon}\right)_J (\bar{\epsilon}, \bar{J}) \quad [45]$$

$$F_2 \triangleq \left(\frac{\partial \mathscr{F}}{\partial J}\right)_\epsilon (\bar{\epsilon}, \bar{J}). \quad [46]$$

F_1 and F_2 are obtained by numerical derivation, $\mathscr{F}$ being computed using the steady-state model [28]. This model is based on the J_G and J_L variables, whereas ϵ and J are used here. The variable change is performed using the drift–flux equations [19] and [23].

The above expressions are substituted in the momentum balance [34], which is then integrated over the riser height using [36], giving

$$\rho_L L(1 - C_0\bar{\epsilon})g''(t) - \rho_L(\bar{V}_G - \bar{V}_L)^2[f'(t) - f'(t-T)]$$
$$- F_2 L g'(t) - (F_1 + \rho_L g)\bar{V}_G[f(t) - f(t-T)] - \tilde{p}_1(t) = 0. \quad [47]$$

2.2.3. *Coupling at the air-injection tee.* For integration along the riser, the gas density is taken at the constant pressure $\bar{p}_m$ [17]. For the coupling terms at the tee, the density is taken at the constant pressure $\bar{p}_T$. Thus, the superficial velocities at the tee and in the riser are related by the following relationships:

$$J_{GT} = \frac{\bar{p}_m}{\bar{p}_T} J_G(z = 0, t) \quad [48]$$

$$J_{LT} = J_L(z = 0, t). \quad [49]$$

From [39] and [40]

$$\tilde{J}_{GT} = \frac{\bar{p}_m}{\bar{p}_T} [\bar{V}_G f'(t) + C_0 \bar{\epsilon} g'(t)] \quad [50]$$

$$\tilde{J}_{LT} = -\bar{V}_G f'(t) + (1 - C_0 \bar{\epsilon}) g'(t) \quad [51]$$

and from [19] and [23]

$$\tilde{\epsilon}_{GT} = K_3 f'(t) + K_4 g'(t) \quad [52]$$

with

$$K_3 \triangleq \frac{\bar{V}_G}{\bar{V}_{GT}} \left[\frac{\bar{p}_m}{\bar{p}_T} (1 - C_0 \bar{\epsilon}_T) + C_0 \bar{\epsilon}_T \right] \quad [53]$$

$$K_4 \triangleq \frac{C_0}{\bar{V}_{GT}} \left[\frac{\bar{p}_m}{\bar{p}_T} (1 - C_0 \bar{\epsilon}_T) \bar{\epsilon} - \bar{\epsilon}_T (1 - C_0 \bar{\epsilon}) \right]. \quad [54]$$

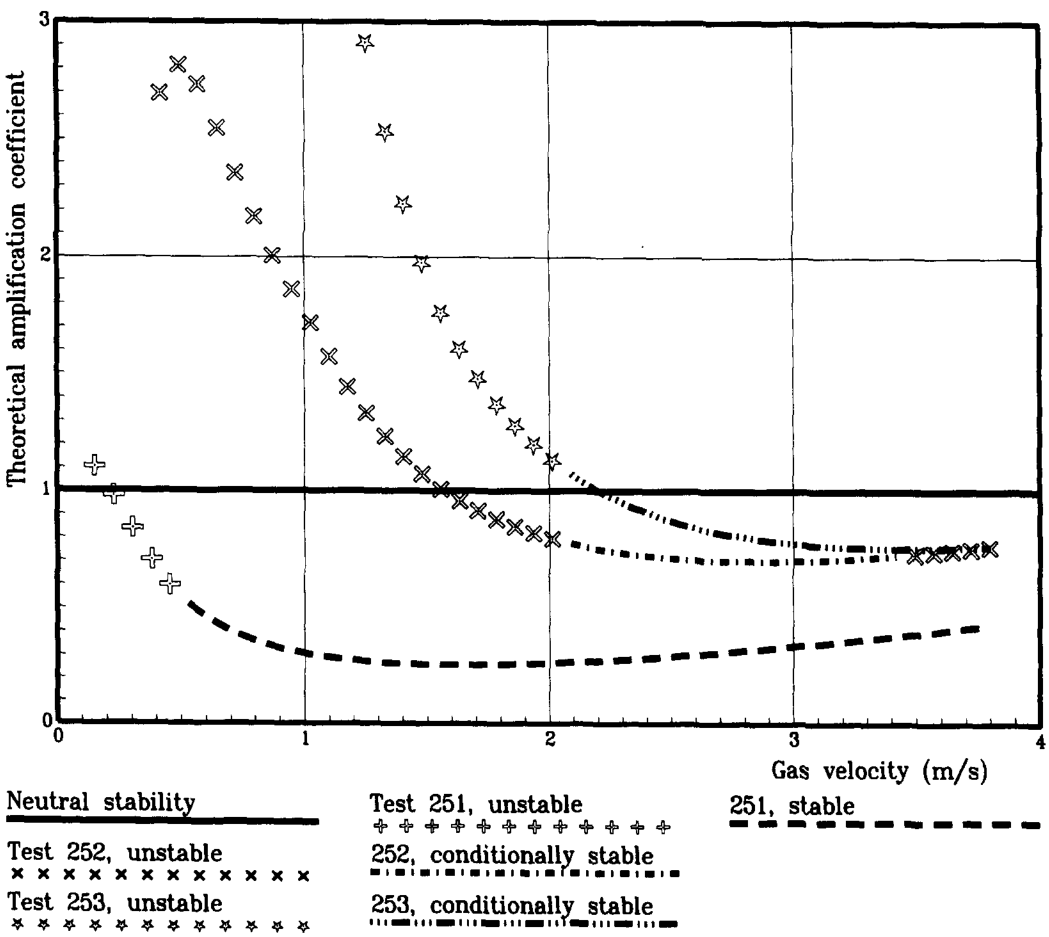

Figure 9. Effect of gas pipe volume on airlift stability.

2.2.4. *The final set of equations.* The expressions for $\tilde{J}_{GT}$, $\tilde{J}_{LT}$, and $\tilde{\epsilon}_T$ are substituted into the single-phase liquid and gas flow equations [29] and [32]. $\tilde{p}_T$ (pressure perturbation at the air-injection tee) is eliminated between the single-phase liquid flow equation [29] and the two-phase flow equation [47], and between the single-phase liquid and gas flow equations [29] and [32].

The following notations are introduced:

$$I_L \triangleq \rho_L L_1 \frac{A}{A_1} \qquad [55]$$

$$I_{LG} \triangleq \rho_L L \qquad [56]$$

$$I \triangleq I_L + I_{LG} \qquad [57]$$

$$G \triangleq \rho_L g \qquad [58]$$

$$\bar{Q}_{GT} \triangleq A \bar{J}_{GT} \qquad [59]$$

$$K_5 \triangleq 1 - C_0 \bar{\epsilon}. \qquad [60]$$

The resulting system of equations describing the evolution of the perturbations f' (void fraction) and g' (mixture superficial velocity) is

$$C_1 f''(t) - C_2 g''(t) + C_3[f'(t) - f'(t-T)] + C_4 f'(t) - C_5 g'(t) + C_6[(f(t) - f(t-T)] = 0 \quad [61]$$

$$C_7 f'''(t) - C_8 g'''(t) + C_9 f''(t) - C_{10} g''(t) + C_{11} f'(t) + C_{12} g'(t) = 0 \qquad [62]$$

with

$$C_1 \triangleq \bar{V}_G I_L$$

$$C_2 \triangleq K_5 I$$

$$C_3 \triangleq \rho_L(\bar{V}_G - \bar{V}_L)^2$$

$$C_4 \triangleq \bar{V}_G K_1 - K_2 K_3$$

$$C_5 \triangleq K_5 K_1 + K_2 K_4 - F_2 L$$

$$C_6 \triangleq \bar{V}_G(F_1 + G)$$

$$C_7 \triangleq \bar{V}_G v_2 I_L$$

$$C_8 \triangleq K_5 v_2 I_L$$

$$C_9 \triangleq v_2(\bar{V}_G K_1 - K_2 K_3) + \gamma \bar{V}_G \bar{Q}_{GT} I_L$$

$$C_{10} \triangleq K_5(v_2 K_1 + \gamma \bar{Q}_{GT} I_L) + v_2 K_2 K_4$$

$$C_{11} \triangleq \gamma[\bar{Q}_{GT}(K_1 \bar{V}_G - K_2 K_3) + \bar{V}_G A \bar{p}_m]$$

$$C_{12} \triangleq \gamma[(1 - K_5) A \bar{p}_m - (K_5 K_1 + K_2 K_4) \bar{Q}_{GT}].$$

2.3. *Stability criterion*

The characteristic equation of the system [61], [62] is

$$P_3(\lambda) P_4(\lambda) - P_5(\lambda)[P_1(\lambda) - P_2(\lambda)\, e^{-\lambda T}] = 0 \qquad [63]$$

with

$$P_1(\lambda) \triangleq C_1\lambda^2 + (C_3 + C_4)\lambda + C_6$$

$$P_2(\lambda) \triangleq C_3\lambda + C_6$$

$$P_3(\lambda) \triangleq C_2\lambda^2 + C_5\lambda$$

$$P_4(\lambda) \triangleq C_7\lambda^2 + C_9\lambda + C_{11}$$

$$P_5(\lambda) \triangleq C_8\lambda^2 + C_{10}\lambda - C_{12}.$$

Let the roots of [63] be denoted by

$$\lambda_i = \psi_i + \mathrm{j}\omega_i. \qquad [64]$$

If any of these roots has a positive real part, the corresponding small perturbation, whose frequency is $\omega_i/(2\pi)$, is amplified, and the system is unstable. If not, the system may also be unstable due to the possible existence of subcritical bifurcations. The occurrence of such instabilities which are not predicted by the linear analysis has been investigated on an experimental basis and will be discussed in the next section.

The algorithm used for the numerical determination of the successive roots of [63] is described in de Cachard (1989).

3. EXPERIMENTS

The experimental set-up was described in our first article (de Cachard and Delhaye 1996, section 2.3, figure 1). It was designed to investigate systematically the influence of the relevant geometrical parameters on the airlift stability.

The inertia term in the liquid suction pipe I_L, defined by [55], can be modified by changing the diameter and/or adding extra sections (the friction term is also affected). The airlift submergence can be changed by moving up or down the upstream tank (which also affects the length of the liquid pipe). The gas compressibility effect can be varied by adding extra pipe lengths between the injection tee and the regulating valve, where the flow is choked.

The values of the geometrical parameters for the tests presented here are listed in table 1.

The experimental investigation of the airlift stability has been based on instantaneous liquid flow rate measurements in the liquid suction pipe. A bidirectional electromagnetic flowmeter with a passband of 0–100 Hz was used. The acquisition frequency was 20 Hz. The frequency spectrum was obtained by Fourier transform. The result is divided by the steady (0 Hz) component, to allow a comparison between different tests. The final result is referred to hereafter as the *relative spectral density*.

4. MODEL ASSESSMENT

The model assessment is based on the amplification coefficient c defined by

$$c \triangleq \exp\left(\frac{2\pi\psi_{\max}}{\omega_{\max}}\right) \qquad [65]$$

where $\psi_{\max}$ denotes the maximum of the real parts of the roots of the characteristic equation [63], and $\omega_{\max}$ the corresponding imaginary part. c is the amplification factor, over one period, of the most destabilizing perturbation. The marginal linear stability corresponds to $c = 1$.

Figure 2 presents the theoretical stability curves, i.e. the amplification coefficient vs the imposed gas flow rate obtained for two different airlift geometries. The experimental results, i.e. stable or unstable operation for given values of the air flow rate, are also indicated. For these results, an experimental stability criterion has been chosen arbitrarily, in terms of relative spectral density. The system is considered as unstable if the relative spectral density of one oscillatory mode or more is greater than 0.1. This criterion correlates well with our visual observations. It corresponds to the point when the flow oscillations become apparent.

More detailed experimental information about the various types of operating points represented in figure 2 is displayed in figures 3 to 6. The time traces of the liquid flow rate show the rapid fluctuations of slug flow. The airlift instabilities induce some low frequency modulations. In the frequency graphs, the predicted amplification coefficients are superimposed on the relative spectral density of the experimental signal. It should be pointed out that the linear analysis performed does not attempt to predict quantitatively the peaks in the experimental spectral density.

Figures 3 to 6 correspond to the various stability behaviours observe in test 151 (see table 1 for geometrical data) for increasing values of the injected gas flow rate.

At low gas flow rate (figure 3), the flow is unstable. Visual observation reveals regular oscillations, with the gas entering periodically the liquid pipe (flow reversal). The flow at the riser outlet is strongly pulsating. When the gas flow rate is increased, the strength of the oscillations decreases. For the operating point presented in figure 4, the flow oscillations are still apparent, but there is no more reverse flow. However, the gas–liquid interface, downstream of the injection tee, fluctuates regularly. Further increasing the gas flow rate first stabilizes the flow (figure 5), and then, suddenly, induces very strong oscillations (e.g. figure 6). In this case, the liquid enters periodically the gas pipe (and vice versa).

In fact, figures 5 and 6 correspond to the same value of the injected gas flow rate. The stable flow regime of figure 5 can be destabilized, for example, by suddenly closing and opening again a valve. The oscillatory regime obtained does not depend on the initial conditions. Such operating points are designated 'conditionally stable' in the stability curves presented. The operating points which are designated 'stable' could not be destabilized.

The frequencies of the system oscillatory modes are well predicted by the linear analysis, provided the oscillations are not too strong (figures 3 to 5). For very strong oscillations, the frequencies are shifted (figure 6).

The linear stability boundaries predicted for test 151 are also quite realistic, as may be seen in figure 2. This is also true for test 352 (same figure), which shows quite a different stability behaviour in the flow rate range investigated. Indeed, for test 352, increasing the injected gas flow rate always tends to stabilize the flow, whereas for test 151 it may also have the opposite effect. These differences in behaviour are well described by the analysis. The effects of the governing parameters are analysed in a more systematic way in figures 7 to 9.

Figure 7 presents the influence of the liquid suction pipe geometry. As indicated in table 1, the experiments presented (tests 152, 252, 352) correspond to increasing inertia (and friction) terms. This stabilizes the flow, as it appears in the experimental results as well as in the analysis. Physically, increasing the inertia tends to lower the resonance frequency in the liquid suction pipe (U tube). As a consequence, the high frequency range (corresponding to high gas velocity, i.e. low transit time in the riser) is stabilized.

Figures 8 and 9 show a stabilizing influence of increasing submergence, and a strong destabilizing influence of increasing gas pipe volume. Again, theoretical and experimental trends are in complete agreement. However, the quantitative prediction of the stability thresholds shows a systematic error, in the nonconservative direction.

5. CONCLUSION

Airlift instabilities are due to density waves oscillations in the two-phase flow section. Depending on the liquid flow inertia, friction terms and on the gas flow compressibility term, the density waves are sustained or not. The effect of the gas compressibility term is preponderant.

The objectives of the linear stability analysis are considered as achieved. Actually, the unstable behaviours observed within the linear stability domain are attributed to some nonlinear effects. This is certainly right when both stable and unstable regimes are observed. It should also be right for the always unstable points observed near the marginal linear stability. In this case, the finite perturbations inherent to the system are sufficient to bring it into a neighbouring, unstable state, and the flow cannot be stabilized.

The linear analysis performed predicts the complex and interacting effects of the geometrical parameters and the gas flow rate well. Subcritical instability has only been observed in regions adjacent to the linear stability boundary. Thus, it is possible, using empirically defined safety margins, to predict airlift stability in a conservative manner. Such an empirical criterion has been derived for engineering purposes. The stability prediction, for a given airlift operating point within the linear stability domain, is based on the first (lowest) oscillatory frequency predicted by the linear analysis for this point. If this frequency is far enough from the equivalent frequency (first oscillatory mode) at the linear stability boundary, the point is predicted as stable.

The following empirical stability criterion (de Cachard 1989) is proposed for practical applications:

$$|\log(f/f_{marg})| > \log[1 + K_e(f_{marg}/f_{max})] \qquad [66]$$

where f is the first oscillatory frequency predicted by the linear analysis for the operating point considered, f_{marg} corresponds to the marginal stability, and f_{max} corresponds to the operating point giving the maximum liquid flow rate; K_e is an empirical factor. Our experimental results correlate very well with $K_e = 0.47$, but the applicability of this purely empirical value to very different operating conditions is questionable.

For practical applications, the use of such empirical criteria will be required until a full transient analysis is performed. The problem is particularly challenging due to the moving boundaries between the single-phase and two-phase flow sections during the oscillations, e.g. when a reverse gas flow takes place in the liquid suction pipe, or when the liquid flow is split between the riser and the gas pipe.

Acknowledgements—This work was done under the auspices of the Direction des Réacteurs Nucléaires in the Département de Thermohydraulique et de Physique.

REFERENCES

Apazidis, N. (1985) Influence of bubble expansion and relative velocity on the performance and stability of an airlift pump. *Int. J. Multiphase Flow* **11**, 459–479.

de Cachard, F. and Delhaye, J. M. (1996) A slug-churn flow model for small-diameter airlift pumps. *Int. J. Multiphase Flow* **22**, 627–649.

de Cachard, F. (1989) Etude théorique et expérimentale des instabilités des systèmes de pompage par air-lift. Thèse de Doctorat, INP Grenoble.

Hjalmars, S. (1973) The origin of instability in airlift pumps. *J. Appl. Mech.* **41**, 399–404.